A twisted bay-substituted quaterrylene phosphorescing in the NIR spectral region

Tanja Miletić,[a,b] Andrea Fermi,[a] Ioannis Papadakis,[c,d] Ioannis Orfanos,[c,d] Nikolaos Karampitsos[c,d] Aggelos Avramopoulos,[e,f] Nicola Demitri,[g] Federica De Leo,[h] Simon J. A. Pope,[a] Manthos G. Papadopoulos,[e] Stelios Couris[c,d] and Davide Bonifazi*[a]

[a] School of Chemistry; Cardiff University; Park Place, CF10 3AT, Cardiff, United Kingdom. E-mail: bonifazid@cardiff.ac.uk

[b] Department of Chemical and Pharmaceutical Sciences, INSTM UdR Trieste, University of Trieste, Piazzale Europa 1, 34127 Trieste, Italy

[c] Department of Physics, University of Patras, 26504 Patras, Greece;

[d] Institute of Chemical Engineering Sciences (ICE-HT), Foundation for Research and Technology-Hellas (FORTH), P.O. Box 1414, Patras 26504, Greece;

[e] Institute of Biology, Medicinal Chemistry and Biotechnology, National Hellenic Research Foundation, 48 Vas. Constantinou Avenue, Athens 11635, Greece;

[f] Department of Computer Engineering, Technological Education Institute (TEI) of Sterea Ellada, Lamia 35100, Greece.

[g] Elettra – Sincrotrone Trieste, S.S. 14 Km 163.5 in Area Science Park, 34149 Basovizza – Trieste, Italy.

[h] San Raffaele Hospital, Scientific Institute-IRCCS, Via Olgettina 60, 20132 Milan, Italy

The preparation of the first soluble quaterrylene derivative featuring peripheral *tert*-butyl substituents and sterically hindering, core-anchored triflate groups has been achieved. This involves a facile synthetic route based on an oxidative coupling of perylene precursors in the presence of H_2O_2 as oxidant. The steric hindrance between the OTf substituents at the central bay position of the quaterrylene board triggers a strong deformation of the central perylene planarity, which forces the quaterrylene platform to adopt a twisted geometry as shown by X-Ray analysis. Exceptionally, photophysical investigations show that the core-twisted quaterrylene phosphoresces in the NIR spectral region at 1716 nm. Moreover, third-order nonlinear optical (NLO) measurments on solutions and thin film containing the relevant molecule showed very large second hyperpolarizability values, as predicted by theoretical calculations at the CAM-B3LYP/6-31G** level of theory, making this material very appealing for photonic applications.

Keywords: quaterrylene • chromophores • cyclodehydrogenation • organic phosphorescent dyes • NIR emitters • polycyclic aromatic hydrocarbons • PAHs

Introduction

Amongst the myriad organic semiconductors, polycyclic aromatic hydrocarbons (PAHs) have unquestionably attracted enormous attention.[1–8] Particularly, rylenes, namely oligo(*peri*-naphthalene)s, that can be regarded as substructures of graphene nanoribbons (GNR),[9] are currently of great interest for their potential use in a wide range of optoelectronic applications.[10–15] The bottom-up covalent synthesis in solution is one of the most exploited strategies for the preparation of well-defined low band gap GNRs with tunable opto-electronic properties.[16–22] Up to now, higher order rylenes such as terrylene, quaterrylene, pentarylene and hexarylene and their dicarboxylic imide derivatives have been synthesized.[14,23–25] Among these, rylenediimides received a lot of attention for their application as light-harvesting materials,[26–30] organic electronics,[31–34] photovoltaics,[35–38] and biomedical sensors[39] among others. The interest for this class of chromophores lies in their exceptional photochemical and thermal stabilities, high electron affinity and mobility, good synthetic accessibility and the possibility to finely tune their optical and redox properties.[14,37] It is well known[34,40–46] that with the introduction of substituents in the bay positions of the rylene core one can significantly influence their structural and functional properties. In particular, different substituents such as amines, cyanides, halogens, aryl or aryloxy groups have been attached at the bay positions of rylenediimides so far,[34,38,47] making those substrates highly versatile molecular modules for functional materials.[47–50] In this context, tetra-substituted derivatives are the most commonly investigated thanks to the lack of different isomeric arrangements in the bay positions and their high solubility originated by the twisted π-system. Recently, *Hariharan* and co-workers also demonstrated the importance of this class of compounds reporting the enhancement of triplet state generation as a result of the core-twisted geometry of perylendiimmide substituted in the bay positions.[42,51] However, to the best of our knowledge, up to the present only a few reports describe the bay-

substitution of higher order rylenes that do not bear imide functionalities on the *peri* position.[16,18,52–55] After the first synthesis of an unsubstituted quaterrylene reported by *Clar* in 1948,[56] the preparation of the first soluble alkyl-functionalized quaterrylene derivatives through alkali-metal induced cyclization of oligonaphthalene precursors was reported by *Müllen* and co-workers in 1990.[57] Important intermediates bearing four solubilizing *tert*-octylphenoxy groups in the bay positions of the perylene core have been reported by the same author in a pivotal work concerning the synthesis of soluble polymer with a poly(*peri*-naphthalene) (PPN) backbone.[54] Recently, the groups of *Wang*[52,53] and *Wu*[55] described an efficient synthetic method toward processable bis-N-annulated quaterrylenes and higher order rylenes. However, such molecules being highly electron-rich are mostly unstable under ambient conditions. A breakthrough in the field has been achieved with the preparation of stable long rylene molecules containing cyclopenta ring-fused perylene as the constituent unit (Figure 1, center).[16] In this work, we describe the synthesis of quaterrylene **1** bearing, for the first time, substituents in the central bay position of the quaterrylene core (Figure 1, right). A facile synthetic route based on an oxidative coupling of perylene precursors in the presence of H_2O_2 as oxidant has been proposed to prepare soluble derivatives featuring peripheral *tert*-butyl substituents and sterically hindering, core-anchored triflate groups. This approach allows us to fully characterize the unique quaterrylene derivative **1** by ^{1}H-, ^{13}C-NMR, UV-Vis and emission spectroscopies and HRMS spectrometry. Exceptionally, we found the system phosphorescing in the NIR spectral region at 77 K. Non-linear optical (NLO) responses of core tetra-substituted quaterrylene **1** were investigated, both in solution and thin film, by the Z-scan technique with 35 ps, 532 nm (Vis) and 1064 (infrared) laser excitation. The molecule showed very large second hyperpolarizabilities, as predicted by theoretical calculations at the CAM-B3LYP/6-31G** level of theory.

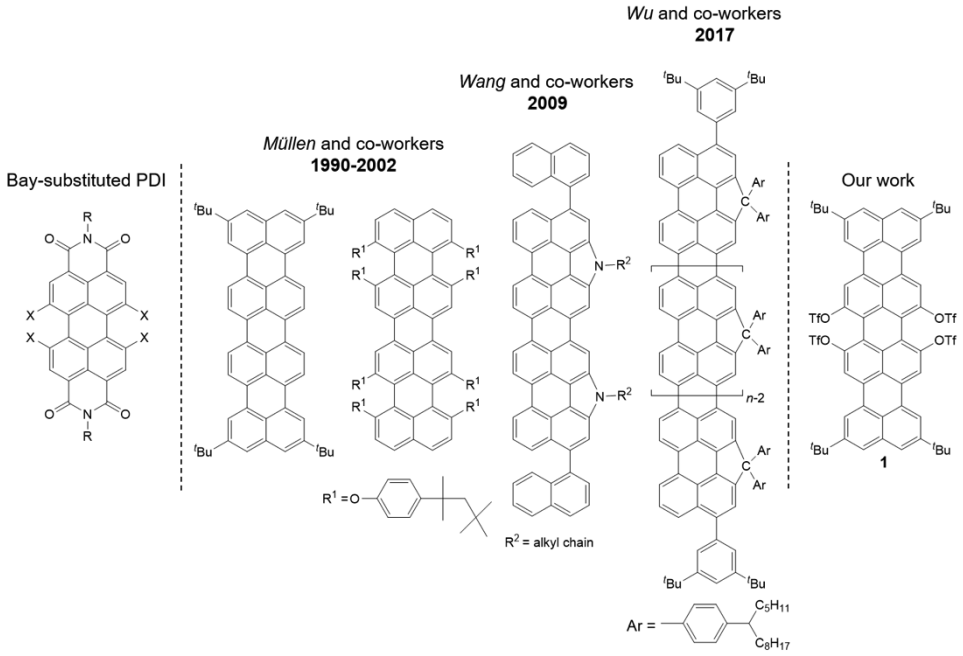

Figure 1. General structure of substituted PAHs at the bay positions: perylenediimine (PDI) (left), rylenes (center) and the core-tetrasubstituted quaterrylene **1** described in this work (right).

Results and Discussion

In our synthetic pathway, the key starting material to obtain core-tetrasubstituted quaterrylene is perylene bis-boronic ester **3,** which was prepared according to a previously reported synthetic protocol.[58,59] Compound **3** was subjected to oxidative hydroxylation to prepare dihydroxyperylene **4** (Scheme 1). Only with the use of a stoichiometric amount of H_2O_2 and NaOH, compound **4** could be successfully isolated in 79 % yield, whereas the use of 6 equivalents of both reactants, oxidant and base, led to the formation of **4** and tetrahydroxy-bisperylene **5** in 36 and 63 % yield, respectively. It is noteworthy to underline that compound **4** is poorly stable even under ambient conditions, undergoing oxidation in solution and on SiO_2, which dramatically affects the reaction reproducibility. Furthermore, we noticed that treating compound **3** with a large excess of oxidant, a complex mixture of products is obtained, which apparently undergoes degradation upon extensive exposure to air. In order to understand the nature of the product formed in the oxidation reaction we performed a triflation reaction (Scheme 1). More specifically, bis-boronic ester **3** was treated with 50 eq. of H_2O_2 (aq. Sol. 35 % wt) in the presence of 50 eq. of NaOH in THF for 24 h. The crude product was directly reacted with triflic anhydride in the presence of DIPEA in CH_2Cl_2. Surprisingly, after four hours we were able to isolate quaterrylene **1** in 16-42% yield, perylene **6** in 9-36% yield and traces of bisperylene **7** (1-2%), all of which very soluble in common organic solvents.

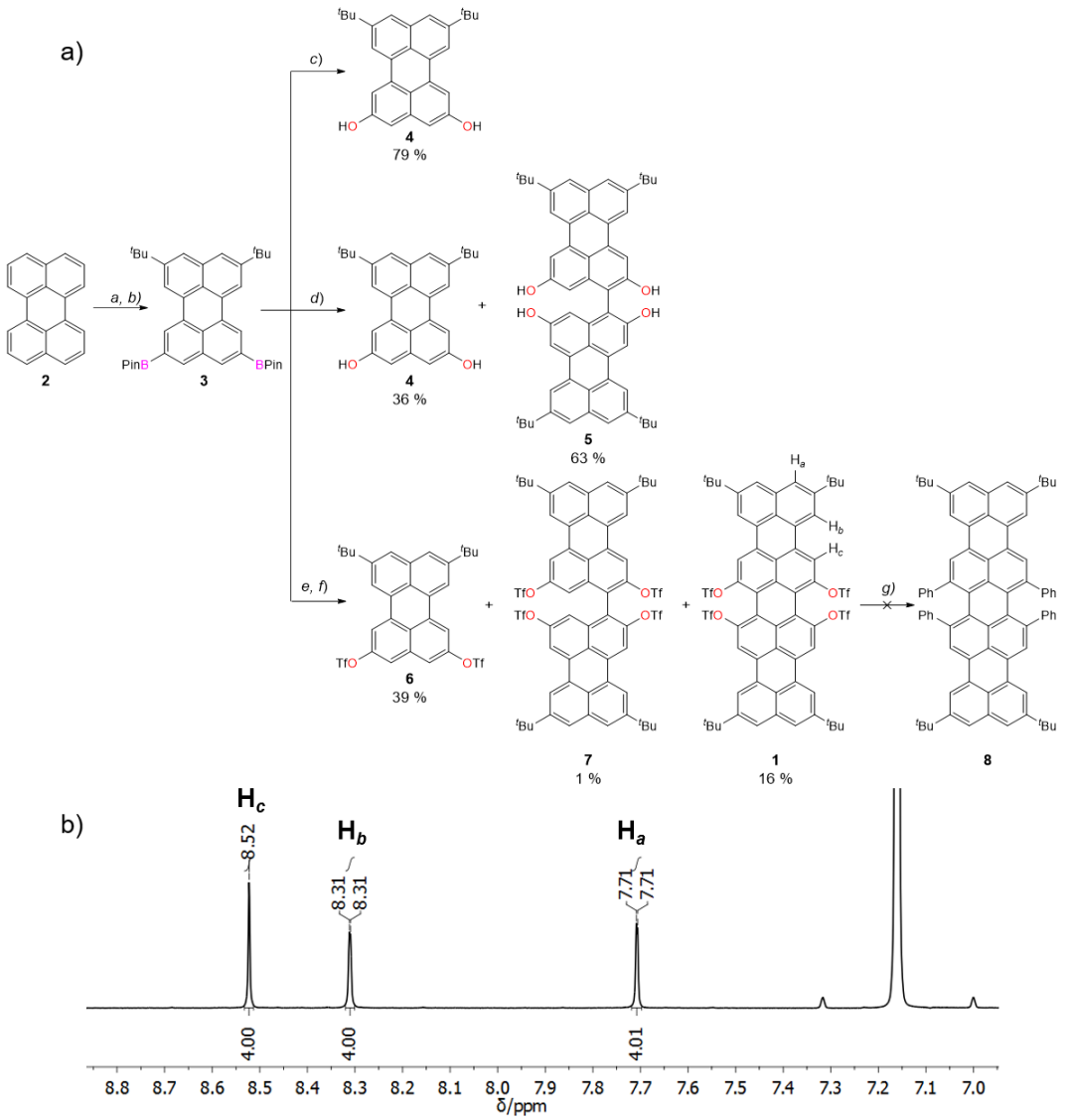

Scheme 1. a) Synthetic route for the preparation of core tetra-substituted quaterrylene. Reagents and conditions: a) $AlCl_3$, *t*BuCl, ODCB, 0 °C to r.t, 24h; b) 10 mol% [{Ir(COD)(OMe)}$_2$], 20 mol% dtbpy, B_2Pin_2, *n*-hexane, 80 °C, 24h; c) NaOH 2 eq. H_2O_2 aq. sol. 30 wt% 2 eq, THF, r.t., 6h; d) NaOH 6 eq. H_2O_2 aq. sol. 35 wt% 6 eq, THF, r.t., 2h; e) NaOH 50 eq., H_2O_2 aq. 35 wt% 50 eq., THF, r.t., 24h. f) DIPEA, OTf_2, CH_2Cl_2, 0 °C to r.t., 4h; g) $Pd(dba)_2$, SPhos, KOAc, Dioxane:H_2O, reflux, 20h. **b)** ^{1}H-NMR spectrum of **1** in C_6D_6 at r.t.

Further attempts to optimize the reaction yields for the oxidation of **3** are reported in Table S1 (SI). Notably, the oxidation reaction with H_2O_2 depicts a certain variability of the yield (Table S2, SI). During these investigations, we figured out that the oxidative homocoupling of molecule **4** also proceeds under air at r.t. in the presence of 2M NaOH. This has been already observed for analogous electron-rich di-hydroxy napthalene derivatives.[60,61] The oxidative C-C bond formation could also have been obtained treating compound **4** with DDQ in the presence of $Sc(OTf)_3$ in toluene for 12 h at r.t and 50 °C (Scheme S2, SI). Analogously to aforementioned, the reaction crude was directly submitted to the trifaltion to isolate compound **1** in 12 and 23% yield, over two steps, respectively. However, no significant amelioration of the reaction yields was achieved. Moreover, when this reaction was performed with PIFA/BF_3·OEt_2 in CH_2Cl_2 at -40 °C[62] molecule **1** was not detected, suggesting that an overoxidation of the substrate took place. In light of these results, we propose a hypotetic mechanism for the oxidative C-C bond formation in Scheme 2. Presumably, we speculate that a deprotonation and a electron abstraction (by either O_2 or the oxidation) are involved generating radical **4**$^{\bullet}$, the latter undergoing radical homocoupling reaction followed by a keto-enol tautomerization to give compound **5**. Most likely, molecule **5** undergoes further oxidation giving radical species **5**$^{\bullet}$, which subsequently experiences an intramolecular radical coupling reaction generating compound **11**, the latter giving tetrahydroxy quaterrylene **12** after tautomerization. Given its electron richness, this substrate seems to be particualry sensitive to oxidation and thus of difficult isolation, as it could give rise to quinone byproducts (**13** and **14**$^{a\text{-}b}$). This hypothesis was confirmed by the fact that quinones **14** (that can have two forms: **14**^{a} and **14**^{b}) could be isolated from the mixture by precipitation from THF/MeOH and characterized by ^{1}H-NMR and HRMS analysis (Figure S15, SI). The ^{1}H NMR spectrum of **14** in DMSO-d_6 consists of one singlet signal at 9.59 ppm (OHs), 6 aromatic peaks in the region between 8.82-7.67 ppm and two singlet signals at 1.54 ppm (*tert*-Butyl groups) in agreement with the tautomeric quinone structure **14** (notably, we could not identify univocally regioisomers **14**^{a} and **14**^{b}). The low intensities of the peaks account for the poor solubility of the

compound in the chosen solvent. HR-MS (MALDI) further confirmed the structure, depicting the peak related to the molecular mass (M) at m/z 786.3732 ($C_{56}H_{50}O_4$, calc.: 786.3709). However, other mechanistic pathways reported, for instance, for the coupling of phenols occurring through a radical cation mechanism cannot be excluded.[63]

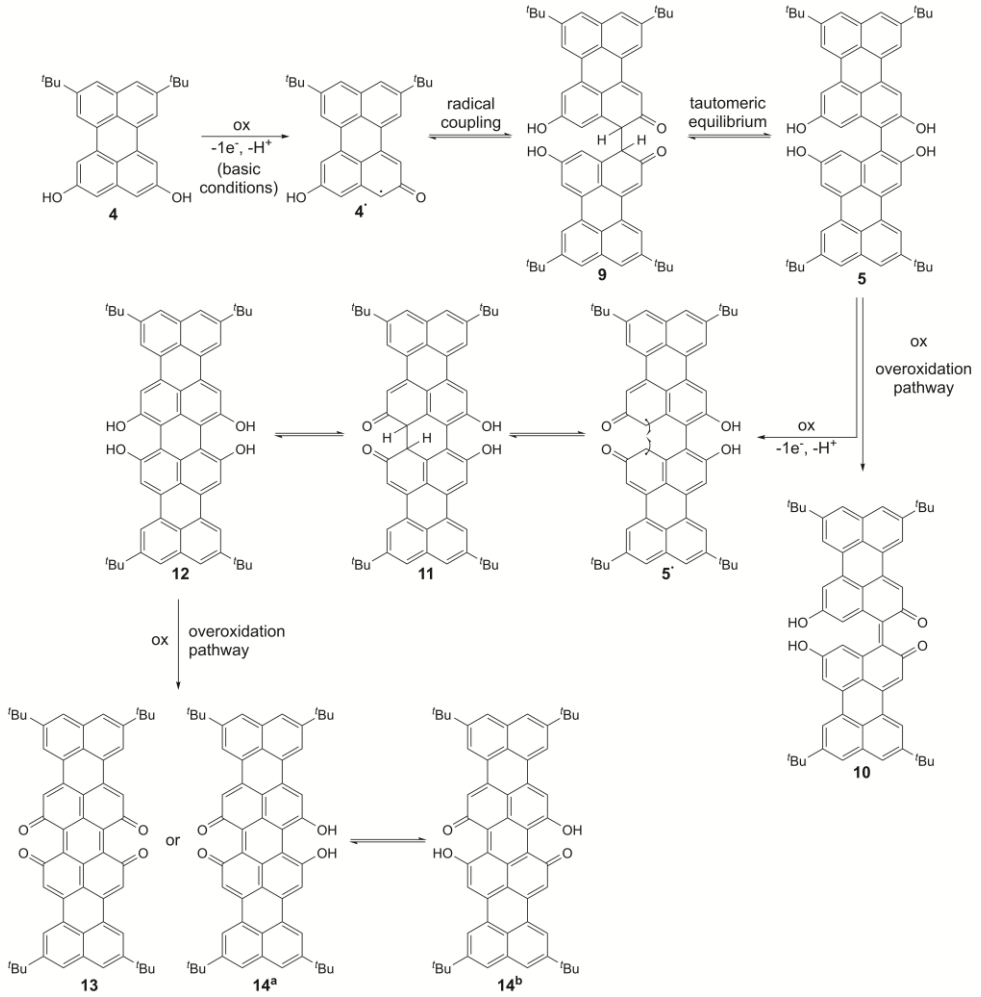

Scheme 2. Proposed mechanism for the oxidative C-C bond formation through a radical pathway.

Finally, different attempts to substitute the four triflate groups in the bay positions of **1** under Suzuki conditions to obtain 8,9,18,19 tetraphenyl quaterrylene **8** were carried out (Scheme 1). Unfortunately, tetra-triflate quaterrylene **1** failed to react with phenylboronic acid following the classical Suzuki–Miyaura coupling route[64] and fluoride ion-mediated and Ag_2O-promoted Suzuki coupling reaction previously described for parent tetrabromoperylene bisimide.[65] In both cases, the cross-coupling reactions lead to an untreatable mixture of products. We speculate that the steric hindrance at the central bay positions of tetra triflate quaterrylene **1** is the limiting factor. The structure of all intermediates and products were unambiguously identified by HR-MS through the detection of the peak corresponding to the molecular mass (M) and by ^{1}H-, ^{13}C- and ^{19}F-NMR, UV-Vis, and IR spectroscopies (see SI, section S3). In particular, for the tetrasubstituted-core derivative **1**, HR-MS (ESI) showed the peak related to the molecular mass (M+1) at m/z 1317.1943 ($C_{60}H_{49}F_{12}O_{12}S_4$, calc.: 1317.1915). Moreover, the ^{1}H NMR characterization of derivative **1** in benzene-d_6, detailed on Scheme 1b, shows a simple spectrum with proton resonances H(*a*), H(*b*), and H(*c*), that appear distinctively as a doublet at 7.71 ppm (J ~ 1.5 Hz), doublet at 8.31 ppm (J ~ 1.5 Hz), and singlet at 8.52 ppm, respectively. The ^{19}F-NMR spectrum (see Figure S12) displays a single peak centered at -73.56 ppm, in agreement with data reported in the literature.[66,67] Although sustained by the spectroscopic and mass spectrometric investigations, only X-ray analysis could unambiguously confirm the molecular structures of both molecules **6** and **1** (Figures 2 and 3). Yellow needle-like crystals suitable for X-ray diffraction analysis of **6** were obtained by slow evaporation of an acetone-d_6 solution. The crystal packing of **6** revealed perylene π–π stacks arranged in pillars along the unit cell axis *b* (Figure 2). Such pillars are tightly packed and the single molecules locked within the pillar through hydrophobic contacts established between the peripheral *t*Bu and OTf substituents. No solvent molecules have been found in the crystal (crystallographic data and refinement details are reported in Table S3, SI).

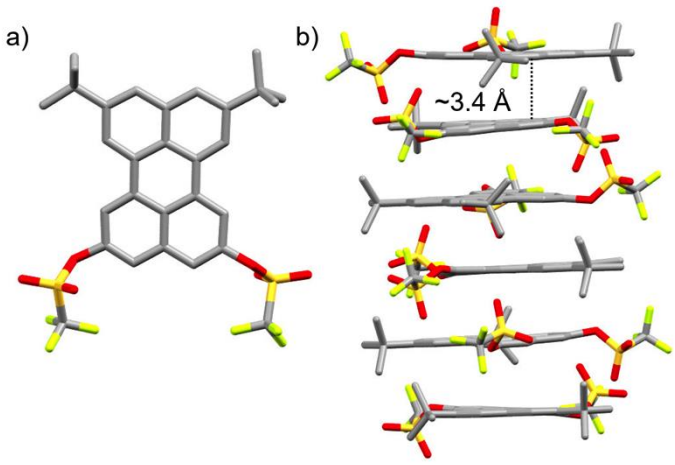

Figure 2. a) X-ray structure and b) side-view of the π-π packing arrangement of ditriflate perylene **6** (space group: *P*nna; atom colors: red O, yellow S, green F, grey C; hydrogens omitted for clarity).

Slow evaporation of a benzene-d_6 solution of quaterrylene **1** yielded dark-blue needle-like crystals suitable for X-ray diffraction analysis (Figure 3 and essential single-crystal refinement data are reported in the SI, Table S3), confirming the formation of the bay-substituted quaterrylene springboard. Clearly, the steric hindrance between the OTf substituents at the central bay position of the quaterrylene board triggers a strong deformation of the central perylene planarity, twisting the naphthyl portions of each perylene units (interplanar angle of ~48°, Figure 3b). This forces the quaterrylene platform to adopt a helicoidal shape, with both the left- and right-handed isomers equally present at the solid state (related by crystallographic inversion centers). The crystal packing shows that only C-H···π and very weak π–π stacking contacts are intramolecularly established at the solid state. As observed with tetrasubstituted perylene derivatives at the bay position[48,68–71] one can postulate that the considerable twisting of the quaterrylene backbone also prevents the formation of strong π–π interactions in solution, thus significantly enhancing the solubility of the molecule in organic solvents. In fact, molecule **1** showed high solubility in a large variety of common organic solvents such as CH_2Cl_2, $CHCl_3$, THF, EtOAc and toluene.

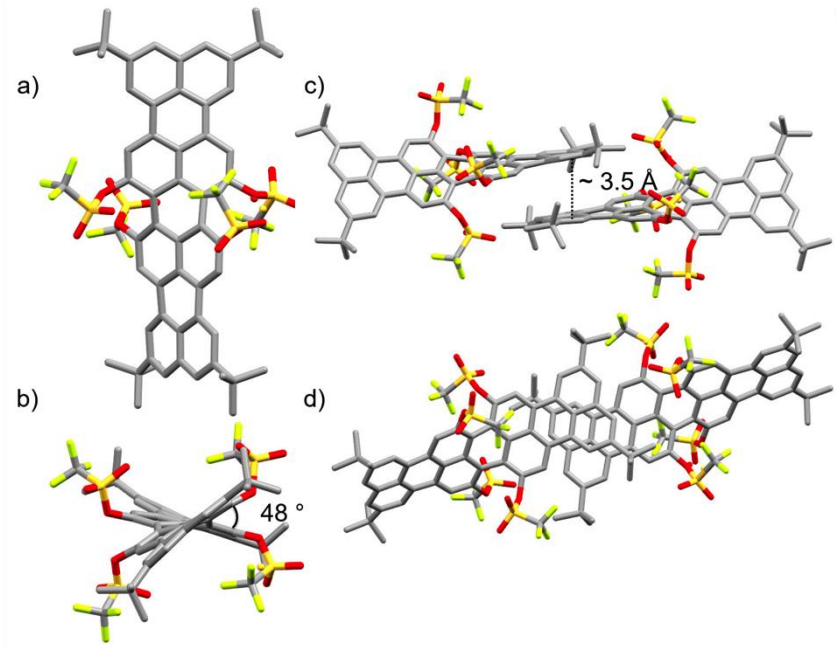

Figure 3. a,d) Top-view and b,c) side-view of the crystal structure and π-π packing arrangement of quaterrylene **1** (space group: *P* $2_1/c$; atom colors: red O, yellow S, green F, grey C; hydrogens omitted for clarity). The interplanar distance is measured in Å and the dihedral angle (Θ) in °.

The thermal stability of compound **1** was investigated by thermogravimetric analysis (TGA). The TGA-DTG profiles of quaterrylene **1** (Figure S18) shows a complex thermal decomposition profile, with a first steep weight loss at 228°C (see the DTG plot) followed by additional two weight losses centered at 265°C and 493°C, respectively. A carbonaceous black residue, representing the 48% of the initial weight, was recovered suggesting that this molecule undergoes some thermal decomposition, most likely triggered by the elimination of the triflate groups.[72]

The photophysical properties of molecule **1** were investigated in toluene solutions and compared with those of ditriflate perylene **6** and tetra *tert*-butyl perylene **9** (Figure 4). Key data are gathered in Table 1. Absorption spectrum of **1** is dramatically red-shifted with respect to molecules **6** and **9**, showing a

broad low energy electronic transition with a maximum at 664 nm (ε = 104600 $M^{-1}cm^{-1}$), similar to that observed for flat unsubstituted quaterrylenes.[73] Consistently, molecule **1** displays a red emission (λ_{max} = 698 nm, 1.78 eV) with a sub-nanosecond lifetime, disclosing a fast deactivation of the singlet excited state. The fluorescence quantum yield (Φ = ~0.04) drops upon the extension of the conjugated π-system within the series **9**>**6**»**1**. Unexpectedly, the increasing distortion of the molecular plane does not affect significantly the emission performance of **1** with respect to its unsubstituted congener previously reported.[74] The phosphorescence spectrum of **1** (using an excitation wavelength of 670 nm) in CH_2Cl_2-MeOH (1:1) glass at 77 K exceptionally showed an unstructured band centered at 1716 nm, while the 77 K fluorescence maximum appeared at 689 nm (Figure 4b). As previously observed for other molecules, these results suggest that the population of the triplet excited state recorded could be induced by the non-planar geometry of molecule **1** as proposed for similar core-twisted PAHs.[42,51,75–78] The corresponding lifetime of **1** at 1720 nm at 77 K appeared to be < 10 ns (*i.e.* beyond the limit of the detector response of our detector). To the best of our knowledge, there are no similar reports in the literature describing such low-energy phosphorescence for PAHs, which appears at higher wavelengths even in comparison with those observed for some organo-lanthanide complexes.[79,80]

Table 1. Optical properties for compounds **1**, **6** and **9** in toluene solutions.

Molecule	λ (nm)[a], ε (M^{-1} cm^{-1})	$\lambda_{max,\,fl}$ (nm)[b]	Φ_F[d]	τ (ns)[e]	$\lambda_{max,\,PH}$ (nm)[f]
9	440, 24300[c]	462	0.93	4.1[g]	-
6	446, 24900	463	0.86	4.3	-
1	664, 104 600	698	0.04	0.9	1716

[a]UV-vis absorption maximum of the lowest energy band in toluene; [b]Emission maximum in air-equilibrated toluene at 25 °C; [c] for **9**, a value of ε = 28 000 M^{-1} cm^{-1} is reported in the literature;[23] [d]Recorded for air equilibrated solutions at 25°C. Coumarin 153 (Φ = 0.53), Rhodamine 6G (Φ = 0.94) and Nile Blue A (Φ = 0.27) in air equilibrated ethanol were used as references for compounds **9**, **6** and **1**, respectively; [e]Fluorescence lifetime (λ_{ex}=355 nm); [f]Recorded in CH_2Cl_2:CH_3OH, 1:1 (v/v) at 77 K: [g]τ = 4.5 ns in EtOH.[81]

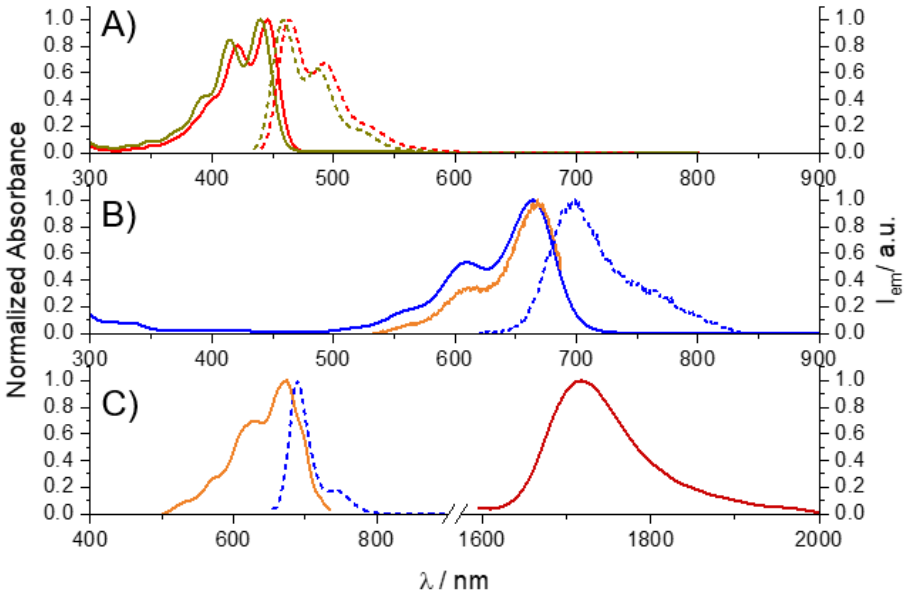

Figure 4. a) Normalized absorption (—) and fluorescence (····) spectra of **9** (dark yellow) and **6** (red) at r.t. in toluene (λ_{ex}=415 nm); b) Normalized absorption (blue), excitation (orange) and fluorescence (blue dotted) spectra of **1** at r.t. in toluene (λ_{ex}=610 nm; λ_{em}=710 nm); c) Normalized excitation (orange, λ_{em}=1720 nm), fluorescence (blue dotted, λ_{ex}=610 nm) and phosphorescence (dark red, λ_{ex}=670 nm) spectra of **1** at 77 K in CH_2Cl_2:CH_3OH (1:1, v/v) rigid matrix.

Furthermore, the electronic properties of core tetra-substituted derivative **1** were studied by cyclic voltammetry (CV) in 1,2-dichlorobenzene (ODCB) (Figure 5), using ferrocene (Fc) as an internal reference. Model compound **6** and extended quaterrylene **1** show one (0.85 V vs. Fc^+/Fc) and two reversible oxidation processes (0.51 and 0.73 V vs. Fc^+/Fc), respectively, while only irreversible processes were detected in the cathodic region (see SI). This is likely to be caused by the presence of triflate substituents, which can undergo an elimination reaction and give rise to irreversible transformations. As previously observed for other rylenes,[14,82] the oxidation potentials are decreasing upon increasing the π-extension of the aromatic scaffold (see molecules **6** and **1**), while the presence of the strong electron-withdrawing triflate substituents tends to deplete the electronic density of the π-cloud. Taken all together, these data allowed us to estimate the energy of the HOMO-LUMO gap of molecule **1** (Figure 6) that results to be 1.80 eV, in good agreement with the computed

results (Table 2). Frontier orbital energies and energy gaps estimated from CV data for molecules **6** and **1** are illustrated in Figure 6, showing a significant shrinking of the HOMO-LUMO gap of **1** as a consequence of the significant extension of the π-surface.

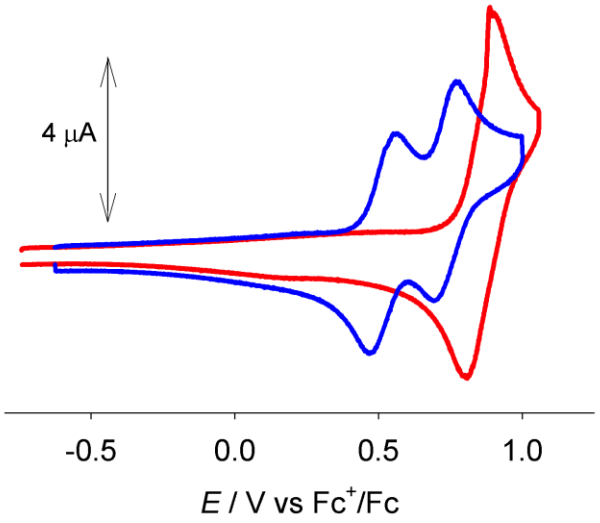

Figure 5. Cyclic voltammetry of **1** (0.45 mM, blue line) and **6** (0.74 mM, red line) in 1,2-dichlorobenzene. Scan rate: 50 mV/s. Supporting electrolyte: $TBAPF_6$. Ferrocene is used as internal reference.

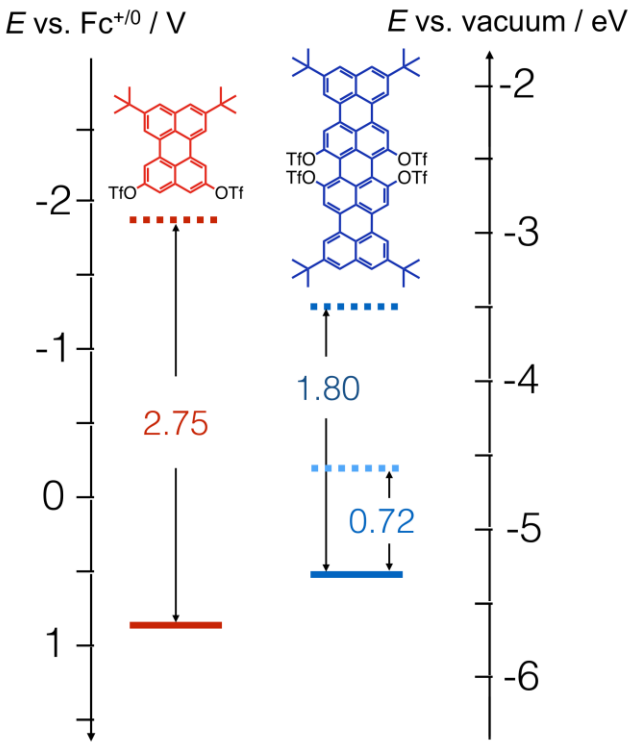

Figure 6. Frontier orbital energies and energy gaps of compounds **1** and **6** estimated from CV data, considering halfwave potentials for oxidations and peak potentials for reductions. Fc+/Fc=−4.8 eV vs. vacuum. Redox potential of the $\mathbf{1}^{\bullet+}/\mathbf{1}^{*T}$ couple, calculated by considering the triplet excited state energy, is also shown.

To shed further light on the electronic structure and optical properties of the triflate substituted perylene derivative, the electronic properties of the HOMO and LUMO levels were calculated performing Density Functional Theory (DFT) calculations using the Gaussian 09 package.[83] Molecule **1** was modeled in its neutral state performing a geometry optimization and a single point calculation using the Restricted Becke's three-parameter exchange functional,[84] the Lee–Yang–Parr correlation functional[85] (B3LYP/6-31G** level of theory). The crystal structure, was considered as the starting geometry. The HOMO and LUMO orbitals were plotted using the Avogadro software.[86] Other orbitals up to HOMO-4 and LUMO+4 were also calculated (Figure 7). It transpires that the molecular HOMO and LUMO orbitals of **1** are located on the entire π–surface of the molecule. Molecular structure of **1** was compared with that of unsubstituted quaterrylene, optimized by using the B3LYP/6-31G** method. The strong deformation of the central perylene core due to the introduction of bulky OTf substituents in central bay positions is evidenced in Figure S24 of the SI, which is in agreement with the geometry of the X-Ray structure (Figure 3).

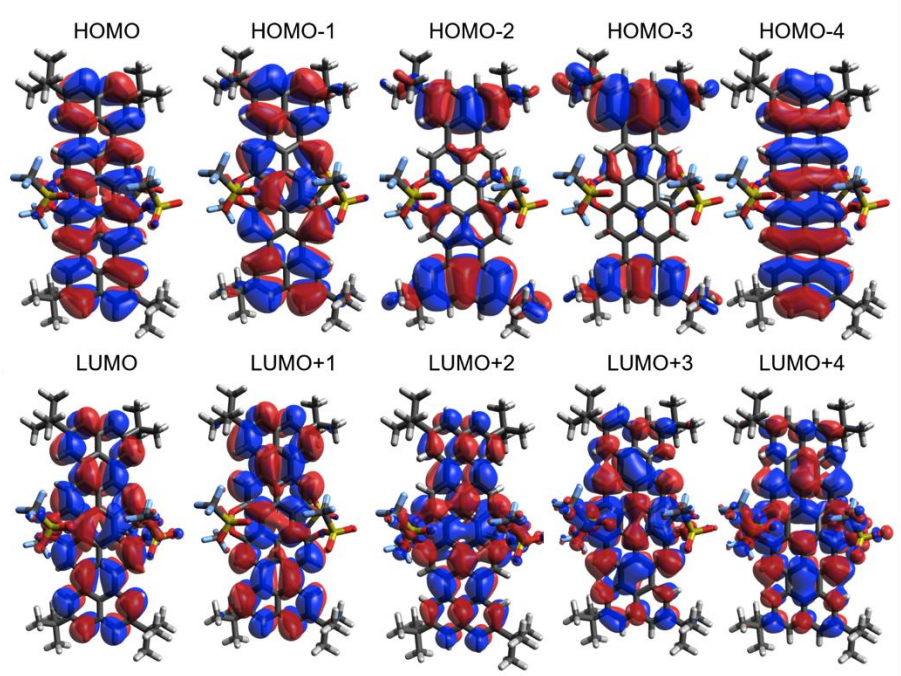

Figure 7. Frontier orbitals of compound **1**, calculated with DFT methods at the B3LYP/6-31G** level of theory.

In addition, the experimental photophysical measurements were compared with those theoretically calculated. The transition energies were computed by employing the time-dependent density functional theory (TD-DFT),[87] using the CAM-B3LYP functional. The computed UV-Vis spectrum of **1** is shown in Figure S25 of the SI and the absorption wavelength λ_{abs} for the first allowed electronic transition is presented in Table 2. For comparison purpose the maximum absorption wavelength λ_{abs} of unsubstituted quaterrylene and the respective UV-Vis spectrum are reported in Table 2 and Figure S26, SI, respectively. The solvent (toluene) effect on the wavelength λ for the first allowed electronic transition was also taken into account in the simulation. The calculated maximum absorption wavelength for molecule **1** is centered at 611 nm which in good agreement with the experimental value ($\lambda_{abs} = 664$ nm, see Figure 4 and Table 1). However, similar spectral characteristics were found for unsubstituted quaterrylene (Figure S26, SI), whereas its λ_{abs} lies at 659.4 nm, implying that the introduction of OTf substituents in the quaterrylene bay positions has a modest effect on the λ_{abs}. Nonetheless, a noticeable difference between the two UV-Vis spectrum is observed. A strong absorption in the UV region, centered at 251 nm, was computed for molecule **1**. In Figure S27, the first allowed electronic transition of **1**, computed with the aid of natural transition orbital pairs,[88] is depicted. One can hardly fail to notice that the electronic transition is assigned to a π -> π* excitation involving the aromatic rings of the quaterrylene. This is confirmed by the computed charge density difference[89] between the ground state and the first dipole-allowed electronic transition of **1** (Figure S28, SI), in which the hole (blue) and electron (red) distributions covering the aromatic rings of the molecule indicate a local excitation.

Table 2. Computed E_{HOMO}, E_{LUMO}, E_{HOMO}-E_{LUMO} ($|HLG|$), absorption wavelength λ (nm), and the excitation energy E_{exc} (eV) for the first allowed electronic transitions of tetra-OTf substituted compound **1** and reference unsubstituted quaterrylene. The values were calculated with the CAM-B3LYP/6-31G**method with explicit solvation (toluene).

Molecule	E_{HOMO} & E_{LUMO}[a] (eV)	$\|HLG\|$[b] (eV)	λ_{abs} (nm)[c]	E_{exc} (eV)[d]	Type of excitation	λ (nm)[f]
1	-5.06 & -3.13	1.93	610.99	2.03	HOMO --> LUMO (96.8%)	664
quaterrylene	-4.38 & -2.56	1.82	659.44	1.88 2.01[g] 2.04[h]	HOMO --> LUMO (96.8%)	

[a]Computed E_{HOMO} and E_{LUMO} potentials, [b]Computed HOMO/LUMO gap; [c]Computed absorption maxima (nm); [d]Computed excitation energy (eV); [f]Experimental UV/Vis absorption maximum of the lowest-energy band in toluene; [g]Ref.[75], Method CASPT2; [h] Referred to the experimental value from Ref.[90]

Furthermore, we have computed the wavelength for the phosphorescence emission of **1**. For this, the geometry of **1** was optimized at the triplet state (B3LYP/6-31G*). The expectation value of the spin operator, $<S^2>$, for the triplet state is equal to 2.06, indicating a negligible spin contamination. It was found that, $\Delta E_{ST} = E_{opt}(T) - E_{opt}(S) = 0.0329\ a.u.\ (1384.8\ nm)$. For the computation of ΔE_{ST} (CAMB3LYP/6-31G*) the effect of the solvent (MeOH) was also considered. The computed value of ΔE_{ST}, is in reasonable agreement with the experimental one (1716 nm, see Figure 4 and Table 1).

The nonlinear optical (NLO) response of molecule **1** has been studied under visible (532 nm) and infrared (1064 nm) 35 ps laser excitation and its NLO properties (*i.e.* NLO absorption and refraction) determined using the Z-scan technique. The NLO response of **1** was studied both, in toluene solution and in thin films of PMMA. The Z-scan is a powerful and relatively simple technique that allows the determination of the magnitude and the sign of the nonlinear absorption coefficient β (m/W) and the nonlinear refractive index parameter, γ' (m^2/W) of a sample, all from a single measurement. Since the Z-scan technique has been presented in detail elsewhere,[91,92] only a brief description will be given hereinafter. According to this technique, the normalized transmittance *T* of a sample is measured by two different experimental configurations, as it is translated along the propagation direction (*e.g.* the z-axis) of a focused Gaussian laser beam. These two experimental configurations are known as "open-aperture" (OA) and "closed-aperture" (CA) Z-scans, respectively. Following the former configuration, the transmitted laser beam through the sample is collected and measured just after the sample, while in the latter, the laser beam is measured after it has passed through a small aperture placed at the far field. The OA Z-scan provides information about the NLO absorption, while the CA Z-scan provides information about the NLO refraction of the sample. Specifically, the shape of the OA Z-scan can exhibit a transmittance minimum or a maximum, corresponding to reverse saturable absorption (RSA) or saturable absorption (SA) behavior of the sample, respectively. On the other hand, the CA Z-scan can present a transmittance minimum followed by a post-focal maximum (*i.e.* a valley-peak configuration), corresponding to self-focusing (the sample acting as a positive/focusing lens) or a peak-valley configuration corresponding to self-defocusing (the sample acting as a negative/defocusing lens).

From the OA Z-scan the nonlinear absorption coefficient β can be determined fitting the experimental transmittance curve by the following equation:[91]

$$T = \frac{1}{\sqrt{\pi}\left(\frac{\beta I_0 L_{eff}}{1 + z^2/z_0^2}\right)} \int_{-\infty}^{+\infty} ln\left[1 + \frac{\beta I_0 L_{eff}}{1 + z^2/z_0^2} exp(-t^2)\right] dt$$

where I_0 is the on-axis peak irradiance, L_{eff} is the effective thickness of the sample given by the relation: $L_{eff} = (1 - e^{-a_0 L})/a_0$, and a_0 is the linear absorption coefficient of the sample at the laser excitation wavelength and L is the thickness of the sample. The α_0 for the solution was obtained through the relation: $\alpha_0(cm^{-1}) = \ln 10 \frac{A\ (au)}{l\ (cm)}$ (with A the absorbance at 532 nm and *l* the thickness of the sample, *i.e.* 0.1 cm). In the case of thin films, the thickness was *l*=423.4 nm, corresponding to an α_0 value of about 1796 cm^{-1}. The corresponding L_{eff} for the solution and the film were about 0.9 mm and 0.4×10^{-3} mm, respectively.

From the CA Z-scan, the NLO refraction parameter γ' can be deduced using the difference of the normalized transmittance between the valley and the peak, the so-called $\Delta T_{p\text{-}v}$ parameter, when NLO absorption is negligible. In the opposite case, in order to remove the effect of the absorption from the NLO refraction (*i.e.* to decouple the two phenomena occuring simultaneously), the "divided" Z-scan is used, which corresponds to the division of the CA Z-scan by the corresponding OA Z-scan. The $\Delta T_{p\text{-}v}$ parameter is related to the NLO refraction parameter γ' of the sample through the following relation:

$$\gamma' = \frac{\sqrt{2}}{k I_0 L_{eff} 0.406\ (1 - S)^{0.25}} \Delta T_{P-V}$$

where $S = 1 - e^{-2r_a^2/w_a^2}$ is the linear transmission of the aperture, r_a and w_a are the radius of the aperture and the beam radius at the aperture, respectively, and *k* is the wavenumber in vacuum.

The nonlinear absorption coefficient β and the nonlinear refractive index parameter γ' are related to the imaginary part ($Im\chi^{(3)}$) and real part ($Re\chi^{(3)}$) of the third-order nonlinear susceptibility $\chi^{(3)}$ through the following relations:

$$Re\chi^{(3)}\ (esu) = 10^{-6} \frac{cn_0^2}{480\pi^2} \gamma'\ (cm^2/W)$$

$$\text{and } Im\chi^{(3)}(esu) = 10^{-7} \frac{c^2 n_0^2}{96\pi^2 \omega} \beta\ (cm/W)$$

With the real and imaginary parts of $\chi^{(3)}$ known, its magnitude can be easily calculated:

$$\chi^{(3)} = \sqrt{(Re\chi^{(3)})^2 + (Im\chi^{(3)})^2}$$

Since the third-order susceptibility $\chi^{(3)}$ depends on the concentration, in order to facilitate the comparisons of the NLO response with other molecules, the second hyperpolarizability γ is often used, which is a molecular property expressing the third-order optical nonlinearity per molecule. It is defined through the following relation:

$$\gamma = \frac{\chi^{(3)}}{NL^4}$$

where *N* is the number of molecules per unit volume, *L* is the Lorenz–Lorentz local field correction factor defined as $L = (n_0^2 + 2)/3$ and n_o is the refractive index of the solvent (ca. 1.496 for toluene) or of the PMMA (1.493) in the case of the thin film.

Results obtained from Z-scan measurements of **1** on toluene solutions at different concentration and on thin PMMA films are gathered in Table 3. The thin film of PMMA containing the relevant dye was prepared by spin coating on glass substrate (thickness of 423 nm, as measured by a stylus profilometer). The detailed film preparation is reported in the SI (section S10). The UV-Vis-NIR absorption spectra of all samples were measured regularly in order to ensure that no unwanted effects, such as *e.g.* aggregation, laser induced photo-degradation, photo-reduction, *etc* have occurred. All samples were found to exhibit remarkable stability both, prior to, and after, laser irradiation. The UV-Vis-NIR absorption spectra of two different toluene solutions and the thin film are shown in Figure S29. The absorption spectrum of the thin film containing molecule **1** was found to exhibit some broadening of the main absorption band in comparison with those of the toluene solutions, suggesting the presence of non-negligible aggregation of the molecule in PMMA. In Figure 8 the "divided" Z-scans of neat toluene and molecule **1** at three different concentrations, namely 0.25, 0.08 and 0.04 mM, measured under 35 ps, 532 nm laser excitation are reported. In all cases a valley-peak transmittance configuration is observed. We noticed that increasing the concentration of **1** an increse in the $\Delta T_{p\text{-}v}$ magnitude is observed, denoting that the solvent (*i.e.* toluene) and molecule **1** have the same sign (*i.e.* positive) refractive nonlinearity. This sign of the $Re\chi^{(3)}$ of **1** is expected according to the two-level system which predicts positive $Re\chi^{(3)}$ when the excitation frequency is higher than the main resonance frequency of the system, that in our case is located at about 611 nm. The opposite is expected to hold (*i.e.* negative $Re\chi^{(3)}$) when the excitation frequency is lower than the resonance frequency.[93] Similar behavior has been reported elsewhere.[94,95]

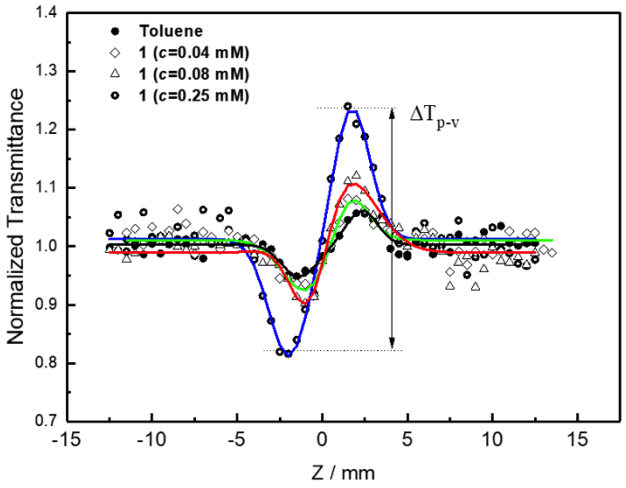

Figure 8. "Divided" Z-scans of neat toluene and molecule **1** in toluene at three different concentrations measured under 35 ps, 532 nm laser excitation.

For toluene solutions and thin film of **1,** the dependence of the $\Delta T_{p\text{-}v}$ parameter as a function of the incident laser energy is shown in Figure 9. From the slopes of the straight lines corresponding to the linear best fit of the experimental data points the nonlinear refractive parameter γ' is deduced and the $Re\chi^{(3)}$ can be calculated from the previously given relations. As can be seen, the thin film exhibits opposite sign nonlinear refractivity, *i.e.* negative $Re\chi^{(3)}$ with respect to those measured in solution (Figure 9b). In fact, the "divided" Z-scans performed on the thin film at several positions and using different laser energies were all found to exhibit a peak-valley configuration, *i.e.* the opposite trend than the solutions. This could be plausibly attributed to the effect of aggregation and/or other intermolecular interactions that **1** undergoes in the thin film. Moreover, as negative control, a solution of PMMA (60 mg/mL) without the relevant dye was spin-coated on a glass substrate. No measurable NLO response, for the range of laser energies employed, was detected. It is noteworthy to underline that both, the toluene solutions at different concentration and the thin film of **1** did not exhibit any measurable NLO absorption under 532 nm excitation, at least up to the double of the range of incident laser energies employed. This experimental finding is extremely promising for several photonic/optoelectronic applications in the visible wavelength range. Z-scan measurements performed under 1064 nm, 35 ps excitation did not show any measurable NLO response for laser energies as high as 15μJ.

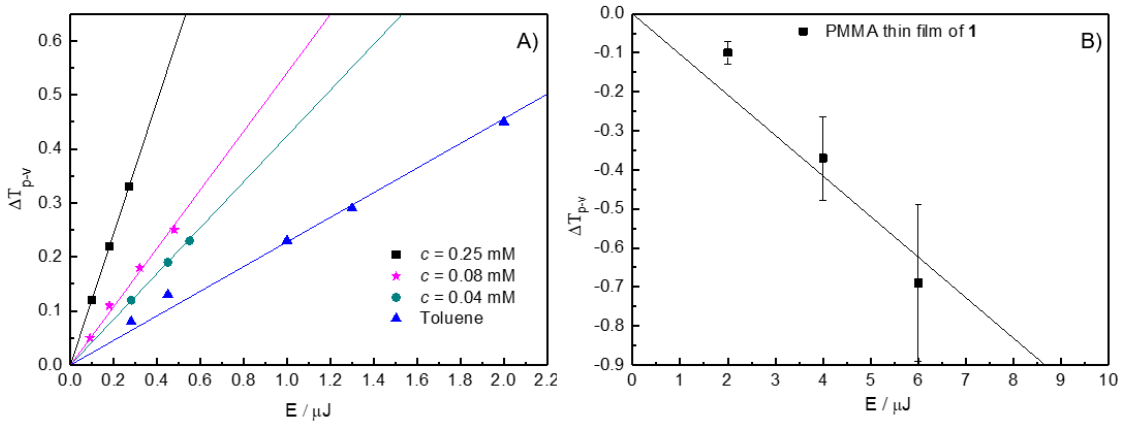

Figure 9. Variation of the $\Delta T_{p\text{-}v}$ parameter as a function of incident laser energy for (a) neat toluene and **1** in toluene (c = 0.25, 0.08 and 0.04 mM), and (b) PMMA thin film containing **1** (1mM in 60 mg/ml PMMA in toluene).

The experimental values of the NLO parameters of molecule **1** in toluene solutions and thin PMMA film are gathered in Table 3. Molecule **1** showed significantly higher NLO second hyperpolarizability values in respect to data reported in the literature for parent π-extended PAHs.[59] Moreover, comparing the values of the NLO parameters of the thin film with those of solutions, it is easily seen that they are exceptionally larger, and, as already mentioned, of opposite sign refractive nonlinearity, *i.e.* negative $Re\chi^{(3)}$. This situation is most probably due to the formation of aggregates favouring larger NLO response and to the change of sign, a situation that is very attractive for several applications in photonics, in particular in the absence of nonlinear absorption. Similar behaviour between the solutions and thin films have been reported recently elsewhere.[96]

Table 3. NLO parameters of **1** in toluene solutions at different concentrations and PMMA thin films on glass under 35 ps, 532 nm laser excitation.

Sample / concentration (mM)	γ' **(×10^{-18} m^2/W)**[b]	$\chi^{(3)}$**(×10^{-13} esu)**[c]	γ **(10^{-31} esu)**[d]
Toluene	1.22±0.03	1.73±0.04	0.73±0.01
1 / 0.25	6.66±0.03	9.45±0.04	15.7±0.2
1 / 0.08	1.86±0.06	2.64±0.09	
1 / 0.04	1.12±0.03	1.59±0.04	
1 in PMMA on glass[a] / 1mM	-1394±134	-1977±190	-

[a] Thin film thickness of 423 nm; [b] NLO refraction parameter; [c] Third-order susceptibility; [d]Second hyperpolarizability.

To further interpret this NLO response, the static electronic (*i.e.* when the excitation frequency of the incoming laser beam tends to zero, with $\omega \to 0$) and frequency-dependent (*i.e.* $\omega \neq 0$) second hyperpolarizabilities, denoted as $\gamma(0;0,0,0)$ and $\gamma(-\omega;\omega,-\omega,\omega)$, respectively, were calculated using the CAM-B3LYP/6-31G** method. Results obtained for molecule **1** were compared with those computed for reference unsubstitued quaterrylene. To all computations the structure of **1** is rotated so that its dipole moment coincides with z-axis. For all the reported second hyperpolarizabilty computations employed for derivative **1**, the *t*-Bu groups have been substituted with H, in order to reduce the computational time. The *t*-Bu groups have a small effect on the value of the average second hyperpolarizability, as shown from a previous study on π-extended PAHs.[59] The results for the static and dynamic second hyperpolarizability, $\gamma(-\omega;\omega,-\omega,\omega)$, of **1** and reference unsubstituted quaterrylene in the gas phase are reported in Table 4. The effect of the solvent, on the frequency-dependent hyperpolarizabilities, has been calculated employing the following approximation:

$$\gamma^{sol}(d) = \rho\gamma^{gas}(d)$$

where γ^{sol}(d) and γ^{gas}(d) denote the $\gamma(-\omega;\omega,-\omega,\omega)$ values of the derivative d, in solution and the gas phase, respectively; while ρ is defined as $\rho=\gamma^{sol}/\gamma^{gas}$, where $\gamma^{sol}(o;o,o,o)$ and $\gamma^{gas}(o;o,o,o)$ are the static second hyperpolarizabilities, computed in the presence of the solvent (toluene) and in the gas phase, respectively. This approximation has been successfuly employed, in several cases, to compute the solvent effect on the hyperpolarizabilities.[59] It has been found that

ρ(**1**) = 0.94 ρ(quaterrylene), thus, the solvent effect on the NLO response of **1** and unsubstituted quaterrylene is similar. It is observed that at the static case (ω=0): γ^{sol}(**1**) = 0.6 γ^{sol}(quaterrylene). It can also be noted that |HLG|^{sol}(**1**) = 2.1 |HLG|^{sol}(quaterrylene). The previous trends show the dependence between $\gamma(o)$ and HLG for **1** and quaterrylene, where the decrease of the HLG leads to an increase of $\gamma(o)$. However, the frequency-dependent results show a different trend: γ^{sol}(**1**) = 11.4γ^{sol}(quaterrylene). This change of the picture could be attributed to the fact that the computed absorption wavelength of **1** (611 nm) lies closer to the excitation wavelength of the laser (532 nm), compared with that of quaterrylene (659.4 nm). The computed $\gamma(-\omega;\omega,-\omega,\omega)$ value of **1** is in good agreement with the experimental data (Table 4). Moreover, in Figure S26 of the SI, it is notable that around the region of the excitation wavelength (532 nm) the absorption (ε) of **1** is almost 1.8 times larger than that of quaterrylene, which could explain the computed higher NLO response of **1**.

Table 4. The average values of static ($\gamma(0)$) and dynamic second-hyperpolarizabilities ($\gamma(-\omega;\omega,-\omega,\omega)$) of core-tetrasubstituted quaterrylene **1** and reference unsubstituted quaterrylene. The reported data were calculated at the B3LYP/6-31G**gas phase optimized geometry, by using the CAM-B3LYP/6-31G** method. The *t*-Bu groups are substituted with H atoms.

Molecule	$\boldsymbol{\rho = \gamma^{sol}/\gamma^{gas}}$ [a]	$\boldsymbol{\gamma(0;0,0,0)}$ $[\times \mathbf{10^3}]$ $(\boldsymbol{a.u.})$	$\boldsymbol{\gamma(-\omega;\omega,-\omega,\omega)}$ [b] $[\times 10^3]$ $(\boldsymbol{a.u.})$	$\boldsymbol{\gamma(-\omega;\omega,-\omega,\omega)}$ $[\times \mathbf{10^{-31}}]$ $(\boldsymbol{esu})$
quaterrylene	2.61	2983[c]	83020[c]	1.09[e,g]
		7780[d]	216682[e]	
1	2.46	1907[c]	1002701[c]	12.4[e,g]
		4692[d]	2466644[e]	15.7±0.2[f]

[a] γ^{sol}:second hyperpolarizability computed in the presence of the solvent (toluene); γ^{gas}:second hyperpolarizability computed in the gas phase. [b] Frequency-dependent value, λ=532 nm. [c] Second hyperpolarizability computed in the gas phase. [d]Value computed in the presence of toluene. [e] Value computed by multiplying the gas-phase value with the scaling factor, ρ, in order to get an estimation of the property value in solution. [f]The experimental value was measured by using the Z-Scan technique, with 35 ps laser excitation at 532 nm (solvent: toluene). [g]The computed value was converted to esu by using the conversion factor 1 a.u.=5.0367 x 10^{-40} esu.

Conclusions

We have described the synthesis of soluble quaterrylene derivative **1** featuring peripheral *tert*-butyl substituents and sterically hindering, core-anchored triflate groups. To this end, a synthetic route based on an oxidative coupling of perylene precursors in the presence of H_2O_2 as oxidant has been employed. X-ray diffraction clearly showed that the steric hindrance between the OTf substituents at the central bay position of the quaterrylene board triggers a strong deformation of the central perylene planarity, twisting the naphthyl portions of each perylene units. Remarkably, this unique core-twisted quaterrylene was found to emit in the NIR spectral region, with a phosporescence maximum centered at 1716 nm at 77K. Considering that, up to now, the library of NIR-emissive organic materials that emit beyond 750 nm is truly limited and it is mostly based on metal complexes[97–102] and chalcogen-containing hybrids,[103,104] this finding is very promising in the design of efficient organic NIR-emitting materials. Moreover, third-order nonlinear optical (NLO) measurments on solutions and thin film containing the relevant dye showed considerably high NLO second hyperpolarizability values (15.7±0.2 × 10^{-31} esu) in comparision with those reported in the literature for parent π-extended PAHs. Particularly, PMMA thin film of core-twisted quaterrylene **1** exhisibits negligible NLO absorption under 532 nm excitation and negative nonlinear refraction making this system very attractive for nonlinear optics and photonics applications. Finally, theoretical computation of the optoelectronic properties performed with the CAM-B3LYP/6-31G** method provided reliable data for predicting the excitation spectra, energy gaps and second hyperpolarisability values corroborating experimental findings. From these results, it becomes evident the importance to further functionalize and/or π-extend the quaterrylene core in order to built a broad variety of emissive molecules. Thus, further investigations will be now focused on studying different strategies to substitute the four triflate groups in the bay positions of **1** in order to finely tune the molecular linear and non-linear optical properties.

Experimental Section

General

Instruments, materials and general methods are detailed in the SI (SI).

Experimental

8,11-di-tert-butylperylene-2,5-diol 4

Perylene bis-boronic ester **3** (1.06 g, 1.72 mmol) and NaOH (137 mg, 3.44 mmol) were dissolved in THF (80 mL). An aqueous solution of H_2O_2 (0.28 mL, 3.44 mmol, 35 wt%) was added drop-wise and the reaction mixture stirred at r.t. for 6 h. The solution was acidified to pH 1-2 by addition of 1 M HCl solution and

extracted with CH_2Cl_2 (3 × 50 mL). Combined organic layers were dried over Na_2SO_4 and the solvent removed in *vacuo*. The crude was purified by column chromatography (neutral Al_2O_3, eluents: EtOAc → EtOAc:MeOH,10:1) affording 8,11-di-tert-butylperylene-2,5-diol (**4**) as a greenish solid (538 mg, 79%). **M.p.**: 204-205 °C. ^{1}**H-NMR** (500 MHz, $(CD_3)_2CO$, 25 °C): δ = 8.52 (s, 2H, O*H*), 8.32 (*d*, ^4J =1.5 Hz, 2H, Ar*H*), 7.80 (*d*, ^4J =2.0 Hz, 2H, Ar*H*), 7.76 (*d*, ^4J =1.5 Hz, 2H, Ar*H*), 6.93 (*d*, ^4J = 2.0 Hz, 2H, Ar*H*), 1.49 (*s*, 18H, C(CH_3)$_3$). ^{13}**C-NMR** (125 MHz, $(CD_3)_2CO$): δ = 157.13, 149.79, 139.53, 135.81, 133.73, 131.01, 126.17, 124.63, 120.16, 119.40, 109.95, 109.27, 35.54, 31.54. **IR** (KBr) ν (cm^{-1}) = 3289, 2953, 2907, 2868, 1605, 1464, 1418, 1393, 1377, 1364, 1340, 1256, 1215, 1173, 1142, 1115, 1070, 1028, 989, 941, 899, 876, 856, 818, 777, 748, 650, 621, 569, 550, 534, 473, 420, 413, 407; **HRMS** (ESI, m/z): $[M+H]^+$ calc. for $C_{28}H_{29}O_2$, 397.2162, found: 397.2158. Compound **4** undergoes oxidation under ambient conditions both, in solution and on SiO_2.

8,8',11,11'-tetra-tert-butyl-[3,3'-biperylene]-2,2',5,5'-tetraol 5

Perylene bis-boronic ester **3** (1.0 g, 1.62 mmol) and NaOH (390 mg, 9.73 mmol) were dissolved in THF (80 mL). An aqueous solution of H_2O_2 (0.836 mL, 9.73 mmol, 35 wt%) was added drop-wise and the reaction mixture stirred at r.t. for 2 h. The solution was acidified to pH 1-2 by addition of 1 M HCl solution and extracted with CH_2Cl_2 (3 × 50 mL). Combined organic layers were dried over Na_2SO_4 and the solvent removed in *vacuo*. The crude was purified by column chromatography (SiO_2, eluents: toluene/EtOAc, 10:0.5) affording 8,11-di-tert-butylperylene-2,5-diol (**5)** as orange solid (402 mg, **63 %**) and compound **4** as greenish powder (232 mg, **36%**). **M.p.**: >300 °C. ^{1}**H-NMR** (500 MHz, $(CD_3)_2CO$): δ = 8.46 (*d*, ^4J = 1.0 Hz, 2H, Ar*H*), 8.41 (*d*, ^4J = 1.5 Hz, 2H, Ar*H*), 8.35 (s, 2H, O*H*), 8.01 (s, 2H, Ar*H*), 7.83-7.82 (*m*, 8H), 6.46 (*d*, ^4J = 2.0 Hz, 2H, Ar*H*), 1.54 (*s*, 18H, C(CH_3)$_3$), 1.52 (*s*, 18H, C(CH_3)$_3$). ^{13}**C-NMR** (125 MHz, $(CD_3)_2CO$): δ =157.44, 155.68, 150.00, 149.97, 138.93, 135.82, 134.07, 133.75, 131.11, 130.98, 126.01, 124.71, 124.69, 120.61, 119.67, 119.50, 114.08, 110.25, 109.93, 108.13, 35.63, 31.57. **IR** (ATR) ν (cm^{-1}) = 3528, 3358, 2955, 2907, 2868, 1601, 1522, 1464, 1437, 1393, 1362, 1341, 1290, 1256, 1209, 1177, 1138, 1069, 993, 945, 878, 856, 820, 777, 766, 733, 644, 621, 590, 503, 417, 405; **HRMS (**ESI, m/z): $[M+H]^+$ calc. for $C_{56}H_{55}O_4$, 791.4095, found: 791.4088; **UV-Vis** (toluene): λ_{max} = 463 nm (ε = 99577 ±1370 M^{-1} cm^{-1}).

Synthesis of 2,5,12,15, tetra-tert-butylquatterylene-8,9,18,19-tetrayl tetrakis(trifluoromethanesulfonate) 1

Perylene bis-boronic ester **3** (100 mg, 0.162 mmol) and NaOH (324 mg, 8.11 mmol) were dissolved in THF (5 mL). An aqueous solution of H_2O_2 (0.7 mL, 8.11 mmol, 35 wt%) was added drop-wise and the reaction mixture stirred at r.t. for 24 h. The solution was acidified to pH 1-2 by addition of 1 M HCl solution and extracted with CH_2Cl_2 (3 ×15 mL). Combined organic layers were dried over Na_2SO_4 and the solvent removed in *vacuo*. The crude was dissolved in anhydrous CH_2Cl_2 (5 mL), and DIPEA (300 µL) was added. The mixture was cooled to 0 °C and Tf_2O (300 µL) added dropwise leading to the formation of an intense blue colored solution. The reaction mixture was allowed to warm up at r.t. and stirred for 4 h under Ar. The organic phase was washed with H_2O (10 mL), aq. 1 M HCl (10 mL), brine (10 mL) and dried over Na_2SO_4. The solvent was removed in *vacuo* and the crude purified by column chromatography (SiO_2, eluents: PET → PET-CH_2Cl_2, 8.5:1.5) to afford compounds **6** (42 mg, **39%**) and **7** (1 mg, **1 %**) as yellow solids and **1** as intense blue solid (17 mg, **16 %**).

8,11-di-tert-butylperylene-2,5-diyl bis(trifluoromethanesulfonate) 6. **M.p.**: 281 °C. ^{1}**H-NMR** (500 MHz, $(CD_3)_2CO$): δ = 8.59 (*d*, ^4J = 1.5 Hz, 2H, Ar*H*), 8.55 (*d*, ^4J = 2.5 Hz, 2H, Ar*H*), 7.97-7.95 (*m*, 4H, Ar*H*), 1.50 (*s*, 18H, C(CH_3)$_3$). ^{13}**C-NMR** (125 MHz, $(CD_3)_2CO$): δ = 150.70, 150.48, 137.26, 136.55, 135.64, 128.90, 128.10, 126.88, 125.46, 121.94, 119.07, 115.48, 35.76, 31.42. **IR** (ATR) ν (cm^{-1}) = 2957, 1609, 1398, 1248, 1205, 1136, 997, 937, 870, 816, 613, 598, 584, 571, 511, 500. **HRMS** (EI, m/z): [M] calc. for $C_{30}H_{26}F_6O_6S_2$, 660.1075, found: 660.1067. **UV-Vis** (toluene): λ_{max}= 446 nm (ε = 24900 M^{-1} cm^{-1}). Crystal suitable for X-ray diffraction was obtained by slow evaporation of solvent from an acetone-d_6 solution (CCDC Number: 1482747; see section S4, SI).

8,8',11,11'-tetra-tert-butyl-[3,3'-biperylene]-2,2',5,5'-tetrayl tetrakis(trifluoromethanesulfonate) 7. M.p.: > 300 °C. ^{1}**H-NMR** (600 MHz, $(CD_3)_2CO$): δ = 8.75-8.73 (*m*, 6H, Ar*H*), 8.71 (*d*, ^4J = 1.2 Hz, 2H, Ar*H*), 8.09 (*d*, ^4J = 1.2 Hz, 2H, Ar*H*), 8.06 (*d*, ^4J = 1.2 Hz, 2H, Ar*H*), 7.31 (*d*, ^4J = 2.4 Hz, 2H, Ar*H*), 1.55 (*s*, 18H, C(CH_3)$_3$), 1.53 (*s*, 18H, C(CH_3)$_3$). ^{13}**C-NMR** (150 MHz, $(CD_3)_2CO$): δ = 151.27, 151.09, 150.94, 149.08, 138.16, 137.15, 136.86, 135.63, 128.84, 128.55, 128.46, 127.80, 127.25, 125.27, 122.78, 122.56, 121.92, 120.55, 120.25, 118.43, 118.13 117.63, 115.92, 115.14, 35.85, 35.83, 31.44, 31.41. ^{19}**F-NMR** (376 MHz, $(CD_3)_2CO$): -74.18, -75.36. **IR** (ATR) ν (cm^{-1}) = 2965, 2872, 1605, 1427, 1248, 1215, 1140, 1007, 943, 881, 818, 608. **HRMS** (ESI, m/z): $[M+H]^+$ calc. for $C_{60}H_{51}F_{12}O_{12}S_4$, 1319.2072, found: 1319.2100.

2,5,12,15, tetra-tert-butylquatterylene-8,9,18,19-tetrayl tetrakis(trifluoromethanesulfonate) 1. **M.p.**: decomposition before reaching the melting point. ^{1}**H-NMR** (500 MHz, C_6D_6): δ = 8.52 (*s*, 4H, Ar*H*), 8.31 (*d*, ^4J = 1.5 Hz, 4H, Ar*H*), 7.71 (*d*, ^4J = 1.5 Hz, 4H, Ar*H*), 1.32 (*s*, 36H, C(CH_3)$_3$); ^{13}**C-NMR** (150 MHz, CD_2Cl_2): δ = 150.92, 147.10, 135.48, 135.30, 135.24, 128.40, 127.82, 126.60, 124.91, 122.45, 122.26, 120.33, 118.20, 117.67, 115.91, 35.70, 31.65. ^{19}**F-NMR** (470 MHz, C_6D_6): δ = -73.56. **IR** (ATR) ν (cm^{-1}) = 2955, 2909, 2870, 1601, 1583, 1568, 1479, 1425, 1410, 1396, 1365, 2905, 1246, 1200, 1173, 1132, 1080, 1055, 1030, 1009, 988, 941, 880, 860, 816, 785, 770, 758, 725, 708, 677, 648, 629, 604, 571, 557, 515, 494, 434, 424, 419, 411. **HRMS** (ESI, m/z): $[M+H]^+$ calc. for $C_{60}H_{49}F_{12}O_{12}S_4$, 1317.1915, found: 1317.1943. **UV-Vis** (toluene): λ_{max}= 664 nm (ε = 104600 M^{-1} cm^{-1}). Crystal suitable for X-ray diffraction was obtained by slow evaporation of solvent from a C_6D_6 solution (CCDC Number: 1482746; see section S4, SI).

Supplementary Material

SI for this article is available on the WWW under http://dx.doi.org/10.1002/MS-number. A summary of crystallographic data are available as ESI asnd the structures deposited with the Cambridge Structural Database (CCD deposition numers: 1482746 and 1482747). These data can be obtained free of charge from The Cambridge Crystallographic Data Centre via www.ccdc.cam.ac.uk/data_request/cif

Acknowledgements

D.B. gratefully acknowledges the EU through Horizon 2020 in particular under the funding scheme Marie Skłodowska-Curie Action-Research and Innovation Staff Exchange (RISE) "INFUSION" project n. 734834 and the Cardiff University. We thank Panagiotis Aloukos for the precious suggestions and help with the NLO analyses on the thin films. Moreover, Prof. Paola Ceroni and Prof. Giacomo Bergamini are kindly acknowledged for the accessability to some equipment of Photochemical Nanoscience Group at University of Bologna.

Author Contribution Statement

T.M. performed all the synthesis and prepared all the materials for the different studies. A.F. performed all the photophysical and electrochemical characterization. S.J.A.P. carried out the phosphorescence lifetime measurements. N.D. performed all the X-Ray diffraction structural characterizations. I. P., I.O., N.K. and S.C. performed all the NLO measurements. A.A. and M.P. performed all the computational studies of the NLO properties and excitation phenomena. F.D.L. perfomed the DFT calculation for the HOMO and LUMO levels. D.B. programmed, designed and coordinated all the scientific activities and wrote the paper through contributions of all authors.

References

[1] J. E. Anthony, 'The Larger Acenes: Versatile Organic Semiconductors', *Angew. Chem. Int. Ed.* **2008**, *47*, 452–483.

[2] X. Feng, W. Pisula, K. Müllen, 'Large Polycyclic Aromatic Hydrocarbons: Synthesis and Discotic Organization', *Pure Appl. Chem* **2009**, *81*, 2203–2224.

[3] J. Wu, W. Pisula, K. Müllen, 'Graphenes as Potential Material for Electronics', *Chem. Rev.* **2007**, *107*, 718–47.

[4] L. Chen, Y. Hernandez, X. Feng, K. Müllen, 'From Nanographene and Graphene Nanoribbons to Graphene Sheets: Chemical Synthesis', *Angew. Chem. Int. Ed.* **2012**, *51*, 7640–7654.

[5] X. Li, X. Wang, L. Zhang, S. Lee, H. Dai, 'Chemically Derived, Ultrasmooth Graphene Nanoribbon Semiconductors', *Science* **2008**, *319*, 1229–1232.

[6] J. Liu, B.-W. Li, Y.-Z. Tan, A. Giannakopoulos, C. Sanchez-Sanchez, D. Beljonne, P. Ruffieux, R. Fasel, X. Feng, K. Müllen, 'Toward Cove-Edged Low Band Gap Graphene Nanoribbons', *J. Am. Chem. Soc.* **2015**, *137*, 6097–6103.

[7] D. Stassen, N. Demitri, D. Bonifazi, 'Extended O-Doped Polycyclic Aromatic Hydrocarbons', *Angew. Chem. Int. Ed.* **2016**, *55*, 5947–5951.

[8] M. Gsänger, D. Bialas, L. Huang, M. Stolte, F. Würthner, 'Organic Semiconductors based on Dyes and Color Pigments', *Adv. Mater.* **2016**, *28*, 3615–3645.

[9] K. Müllen, 'Evolution of Graphene Molecules: Structural and Functional Complexity as Driving Forces behind Nanoscience', *ACSNano* **2014**, *8*, 6531–6541.

[10] W. Zhou, Y. Wen, L. Ma, Y. Liu, X. Zhan, 'Conjugated Polymers of Rylene Diimide and Phenothiazine for n-Channel Organic Field-Effect Transistors', *Macromolecules* **2012**, *45*, 4115–4121.

[11] W. Yue, A. Lv, J. Gao, W. Jiang, L. Hao, C. Li, Y. Li, L. E. Polander, S. Barlow, W. Hu, S. Di Motta, F. Negri, S. R. Marder, Z. Wang, 'Hybrid Rylene Arrays via Combination of Stille Coupling and C–H Transformation as High-Performance Electron Transport Materials', *J. Am. Chem. Soc.* **2012**, *134*, 5770–5773.

[12] W. Jiang, Y. Li, Z. Wang, 'Tailor-Made Rylene Arrays for High Performance n-Channel Semiconductors', *Acc. Chem. Res.* **2014**, *47*, 3135–3147.

[13] X. Guo, D. Tu, X. Liu, 'Recent Advances in Rylene Diimide Polymer Acceptors for All-Polymer Solar Cells', *J. Energy Chem.* **2015**, *24*, 675–685.

[14] T. Weil, T. Vosch, J. Hofkens, K. Peneva, K. Müllen, 'The Rylene Colorant Family—Tailored Nanoemitters for Photonics Research and Applications', *Angew. Chem. Int. Ed.* **2010**, *49*, 9068–9093.

[15] J. H. Jung, M. J. Yoon, J. W. Lim, Y. H. Lee, K. E. Lee, D. H. Kim, J. H. Oh, 'Phototransistors: High-Performance UV–Vis–NIR Phototransistors Based on Single-Crystalline Organic Semiconductor–Gold Hybrid Nanomaterials', *Adv. Funct. Mater.* **2017**, *27*, 1604528.

[16] W. Zeng, H. Phan, T. S. Herng, T. Y. Gopalakrishna, N. Aratani, Z. Zeng, H. Yamada, J. Ding, J. Wu, 'Rylene Ribbons with Unusual Diradical Character', *Chem* **2017**, *2*, 81–92.

[17] T. H. Vo, M. Shekhirev, D. A. Kunkel, M. D. Morton, E. Berglund, L. Kong, P. M. Wilson, P. A. Dowben, A. Enders, A. Sinitskii, 'Large-Scale Solution Synthesis of Narrow Graphene Nanoribbons', *Nat. Commun.* **2014**, *5*, 3189.

[18] W. Yang, A. Lucotti, M. Tommasini, W. A. Chalifoux, 'Bottom-Up Synthesis of Soluble and Narrow Graphene Nanoribbons Using Alkyne Benzannulations', *J. Am. Chem. Soc.* **2016**, *138*, 9137–9144.

[19] M. G. Schwab, A. Narita, Y. Hernandez, T. Balandina, K. S. Mali, S. De Feyter, X. Feng, K. Müllen, 'Structurally Defined Graphene Nanoribbons with High Lateral Extension', *J. Am. Chem. Soc.* **2012**, *134*, 18169–18172.

[20] A. Narita, X. Feng, Y. Hernandez, S. A. Jensen, M. Bonn, H. Yang, I. A. Verzhbitskiy, C. Casiraghi, M. R. Hansen, A. H. R. Koch, G. Fytas, O. Ivasenko, B. Li, K. S. Mali, T. Balandina, S. Mahesh, S. De Feyter, K. Müllen, 'Synthesis of Structurally Well-Defined and Liquid-Phase-Processable Graphene Nanoribbons', *Nat. Chem.* **2014**, *6*, 126–132.

[21] X. Yang, X. Dou, A. Rouhanipour, L. Zhi, H. J. Räder, K. Müllen, 'Two-Dimensional Graphene Nanoribbons', *J. Am. Chem. Soc.* **2008**, *130*, 4216–4217.

[22] A. Narita, X.-Y. Wang, X. Feng, K. Müllen, 'New Advances in Nanographene Chemistry', *Chem. Soc. Rev.* **2015**, *44*, 6616–6643.

[23] J. T. Markiewicz, F. Wudl, 'Perylene, Oligorylenes, and Aza-Analogs', *ACS Appl. Mater. Interfaces* **2015**, *7*, 28063–28085.

[24] L. Chen, C. Li, K. Müllen, 'Beyond Perylene Diimides: Synthesis, Assembly and Function of Higher Rylene Chromophores', *J. Mater. Chem. C* **2014**, *2*, 1938.

[25] T. Heek, F. Würthner, R. Haag, 'Synthesis and Optical Properties of Water-Soluble Polyglycerol-Dendronized Rylene Bisimide Dyes', *Chem. - A Eur. J.* **2013**, *19*, 10911–10921.

[26] H. Langhals, 'Control of the Interactions in Multichromophores: Novel Concepts. Perylene Bis-imides as Components for Larger Functional Units', *Helv. Chim. Acta*

2005, *88*, 1309–1343.

[27] H. Wolf-klein, C. Kohl, K. Mullen, H. Paulsen, 'Biomimetic Model of a Plant Photosystem Consisting of a Recombinant Light-Harvesting Complex and a Terrylene Dye', *Angew. Chem. Int. Ed.* **2002**, *41*, 3378–3380.

[28] R. S. Loewe, K. Tomizaki, W. J. Youngblood, Z. Bo, J. S. Lindsey, 'Synthesis of Perylene–Porphyrin Building Blocks and Rod-like Oligomers for Light-Harvesting Applications', *J. Mater. Chem.* **2002**, *12*, 3438–3451.

[29] P. Schlichting, 'A Bichromophore Based on Perylene and Terrylene for Energy Transfer Studies at the Single-Molecule Level', *Chem. Eur. J.* **1999**, *5*, 2388–2395.

[30] L. Maggini, D. Bonifazi, 'Hierarchised Luminescent Organic Architectures: Design, Synthesis, Self-assembly, Self-organisation and Functions', *Chem. Soc. Rev.* **2012**, *41*, 211–241.

[31] X. Zhan, A. Facchetti, S. Barlow, T. J. Marks, M. A. Ratner, M. R. Wasielewski, S. R. Marder, 'Rylene and Related Diimides for Organic Electronics', *Adv. Mater.* **2011**, *23*, 268–284.

[32] C. Liu, Z. Liu, H. T. Lemke, H. N. Tsao, R. C. G. Naber, Y. Li, K. Banger, K. Müllen, M. M. Nielsen, H. Sirringhaus, 'High-Performance Solution-Deposited Ambipolar Organic Transistors Based on Terrylene Diimides', *Chem. Mater.* **2010**, *22*, 2120–2124.

[33] M. Schneider, J. Hagen, D. Haarer, K. Müllen, 'Novel Electroluminescent Devices Based on Perylene-Doped Sol–Gel Layers', *Adv. Mater.* **2000**, *12*, 351–354.

[34] C. Huang, S. Barlow, S. R. Marder, 'Perylene-3,4,9,10-tetracarboxylic Acid Diimides: Synthesis, Physical Properties, and Use in Organic Electronics', *J. Org. Chem.* **2011**, *76*, 2386–2407.

[35] H. Langhals, S. Christian, A. Hofer, 'Substitution of Aromatics by Amines at Room Temperature with Negative Energy of Activation: Amino peri-Arylenes as Metal-Free Components for Dye-Sensitized Solar Cells', *J. Org. Chem.* **2013**, *78*, 9883–9891.

[36] Y. Lin, X. Zhan, 'Non-Fullerene Acceptors for Organic Photovoltaics: An Emerging Horizon', *Mater. Horiz.* **2014**, *1*, 470–488.

[37] P. Sonar, J. P. Fong Lim, K. L. Chan, 'Organic Non-Fullerene Acceptors for Organic Photovoltaics', *Energy Environ. Sci.* **2011**, *4*, 1558–1574.

[38] C. Li, H. Wonneberger, 'Perylene Imides for Organic Photovoltaics: Yesterday, Today, and Tomorrow', *Adv. Mater.* **2012**, *24*, 613–636.

[39] M. Sun, K. Müllen, M. Yin, 'Water-Soluble Perylenediimides: Design Concepts and Biological Applications', *Chem. Soc. Rev.* **2016**, *45*, 1513–1528.

[40] Y. Li, W. Xu, S. Di Motta, F. Negri, D. Zhu, Z. Wang, 'Core-Extended Rylene Dyes via Thiophene Annulation', *Chem. Commun.* **2012**, *48*, 8204.

[41] Z. Chen, M. G. Debije, T. Debaerdemaeker, P. Osswald, F. Würthner, 'Tetrachloro-substituted Perylene Bisimide Dyes as Promising n-Type Organic Semiconductors: Studies on Structural, Electrochemical and Charge Transport Properties', *ChemPhysChem* **2004**, *5*, 137–140.

[42] K. Nagarajan, A. R. Mallia, V. S. Reddy, M. Hariharan, 'Access to Triplet Excited State in Core-Twisted Perylenediimide', *J. Phys. Chem. C* **2016**, *120*, 8443–8450.

[43] M. Queste, C. Cadiou, B. Pagoaga, L. Giraudet, N. Hoffmann, 'Synthesis and Characterization of 1,7-disubstituted and 1,6,7,12-tetrasubstituted perylenetetracarboxy-3,4:9,10-diimide Derivatives', *New J. Chem.* **2010**, *34*, 2537–2545.

[44] M. Schulze, M. Philipp, W. Waigel, D. Schmidt, F. Wurthner, 'Library of Azabenz-Annulated Core-Extended Perylene Derivatives with Diverse Substitution Patterns and Tunable Electronic and Optical Properties', *J. Org. Chem.* **2016**, *81*, 8394–8405.

[45] A. Fin, I. Petkova, D. A. Doval, N. Sakai, E. Vauthey, S. Matile, 'Naphthalene- and Perylenediimides with Hydroquinones, Catechols, Boronic Esters and Imines in the Core', *Org. Biomol. Chem.* **2011**, *9*, 8246–8252.

[46] F. N. Miros, S. Matile, 'Core-Substituted Naphthalenediimides: LUMO Levels Revisited, in Comparison with Preylenediimides with Sulfur Redox Switches in the Core', *ChemistryOpen* **2016**, *5*, 219–226.

[47] F. Würthner, 'Perylene Bisimide Dyes as Versatile Building Blocks for Functional Supramolecular Architectures', *Chem. Commun.* **2004**, 1564–1579.

[48] F. Würthner, 'Bay-Substituted Perylene Bisimides: Twisted Fluorophores for Supramolecular Chemistry', *Pure Appl. Chem.* **2006**, *78*, 2341–2349.

[49] D. Görl, X. Zhang, V. Stepanenko, F. Würthner, 'Supramolecular Block Copolymers by Kinetically Controlled Co-Self-Assembly of Planar and Core-Twisted Perylene Bisimides', *Nat. Commun.* **2015**, *6*, 7009.

[50] T. E. Kaiser, V. Stepanenko, F. Würthner, 'Fluorescent J-Aggregates of Core-Substituted Perylene Bisimides: Studies on Structure–Property Relationship, Nucleation–Elongation Mechanism, and Sergeants-and-Soldiers Principle', *J. Am. Chem. Soc.* **2009**, *131*, 6719–6732.

[51] K. Nagarajan, A. R. Mallia, K. Muraleedharan, M. Hariharan, 'Enhanced intersystem crossing in core-twisted aromatics', *Chem. Sci.* **2017**, *8*, 1776–1782.

[52] Y. Li, J. Gao, S. Di Motta, F. Negri, Z. Wang, 'Tri-N-annulated Hexarylene: An Approach to Well-Defined Graphene Nanoribbons with Large Dipoles', *J. Am. Chem. Soc.* **2010**, *132*, 4208–4213.

[53] Y. Li, Z. Wang, 'Bis-N-Annulated Quaterrylene: An Approach to Processable Graphene Nanoribbons', *Org. Lett.* **2009**, *11*, 1385–1387.

[54] C. Former, S. Becker, A. C. Grimsdale, K. Müllen, 'Cyclodehydrogenation of Poly(perylene) to Poly(quaterrylene): Toward Poly(peri-naphthalene)', *Macromolecules* **2002**, *35*, 1576–1582.

[55] Q. Qi, P. M. Burrezo, H. Phan, T. S. Herng, T. Y. Gopalakrishna, W. Zeng, J. Ding, J. Casado, J. Wu, 'Ambient Stable Radical Cations, Diradicaloid π-Dimeric Dications, Closed-Shell Dications, and Diradical Dications of Methylthio-Capped Rylenes', *Chem. - A Eur. J.* **2017**, *23*, 7595 –7606.

[56] E. Clar, 'Das Kondensationsprinzip, ein einfaches neues Prinzip im Aufbau der aromatischen Kohlenwasserstoffe (Aromatische Kohlenwassertoffe XLII. Mitteilung)', *Chem. Ber.* **1948**, *81*, 52–63.

[57] A. Bohnen, K.-H. Koch, W. Lüttke, K. Müllen, 'Oligorylene as a Model for "Poly(perinaphthalene)', *Angew. Chem. Int. Ed.* **1990**, *29*, 525–527.

[58] 'Blue light emitting material', J. Pillow, S. Kobayashi, M. Humphries, WO2010/013006 A2, **2010**.

[59] T. Miletić, A. Fermi, I. Orfanos, A. Avramopoulos, F. De Leo, N. Demitri, G. Bergamini, P. Ceroni, M. G. Papadopoulos, S. Couris, D. Bonifazi, 'Tailoring Colors by O Annulation of Polycyclic Aromatic Hydrocarbons', *Chem. - A Eur. J.* **2017**, *23*, 2363 –2378.

[60] J. S. Calderon, R. H. Thomson, 'Autoxidation of Naphthols: a New Entry to the Perylene System', *J. Chem. Soc. Perkin trans. I* **1988**, 583–586.

[61] T. Qiu, H. Wei, D. Cheng, L. Zhang, C. Jiang, S. Luo, L. Yuan, Z. Zeng, 'Towards Perylenequinonoid: Effective Application to Reversible Fluorescent Probe for Monitoring Hydrogen Persulfide in Solvents And Living Cells', *Talanta* **2017**, *164*, 529–533.

[62] T. Takada, M. Arisawa, M. Gyoten, R. Hamada, H. Tohma, Y. Kita, 'Oxidative Biaryl Coupling Reaction of Phenol Ether Derivatives Using a Hypervalent Iodine(III) Reagent', *J. Org. Chem.* **1998**, *63*, 7698–7706.

[63] M. Grzybowski, K. Skonieczny, H. Butenschön, D. T. Gryko, 'Comparison of Oxidative Aromatic Coupling and the Scholl Reaction', *Angew. Chem. Int. Ed.* **2013**, *52*, 9900–9930.

[64] T. Fujikawa, Y. Segawa, K. Itami, 'Synthesis, Structures, and Properties of π-Extended Double Helicene: A Combination of Planar and Nonplanar π-Systems', *J. Am. Chem. Soc.* **2015**, *137*, 7763–7768.

[65] W. Qiu, S. Chen, X. Sun, Y. Liu, D. Zhu, 'Suzuki Coupling Reaction of 1,6,7,12-Tetrabromoperylene Bisimide', *Org. Lett.* **2006**, *8*, 867–870.

[66] F. Gelat, J.-F. Lohier, A.-C. Gaumont, S. Perrio, 'tert-Butyl Sulfoxides: Key Precursors for Palladium-Catalyzed Arylation of Sulfenate Salts', *Adv. Synth. Catal.* **2015**, *357*, 2011–2016.

[67] T. H. Wöste, M. Oestreich, 'BINAP versus BINAP(O) in Asymmetric Intermolecular Mizoroki–Heck Reactions: Substantial Effects on Selectivities', *Chem. - A Eur. J.* **2011**, *17*, 11914–11918.

[68] F. Würthner, P. Osswald, R. Schmidt, T. E. Kaiser, H. Mansikkamäki, M. Könemann, 'Synthesis and Optical and Electrochemical Properties of Core-Fluorinated Perylene Bisimides', *Org. Lett.* **2006**, *8*, 3765–3768.

[69] F. Würthner, A. Sautter, C. Thalacker, 'Substituted Diazadibenzoperylenes: New Functional Building Blocks for Supramolecular Chemistry', *Angew. Chem. Int. Ed.* **2000**, *39*, 1243–1245.

[70] P. Osswald, D. Leusser, D. Stalke, F. Würthner, 'Perylene Bisimide Based Macrocycles: Effective Probes for the Assessment of Conformational Effects on Optical Properties', *Angew. Chem. Int. Ed.* **2005**, *44*, 250–253.

[71] F. Würthner, V. Stepanenko, Z. Chen, C. R. Saha-Möller, N. Kocher, D. Stalke, 'Preparation and Characterization of Regioisomerically Pure 1,7-Disubstituted Perylene Bisimide Dyes', *J. Org. Chem.* **2004**, *69*, 7933–7939.

[72] F. Cataldo, O. Ursini, G. Angelini, S. Iglesias-Groth, 'On the Way to Graphene: The Bottom-Up Approach to Very Large PAHs Using the Scholl Reaction', *Fullerenes, Nanotub. Carbon Nanostruct.* **2011**, *19*, 713–725.

[73] K. H. Koch, U. Fahnenstich, M. Baumgarten, K. Müllen, 'Polynaphthylenes and Oligorylenes, Soluble Electrophores and Chromophores', *Synth. Met.* **1991**, *42*, 1619–1622.

[74] K.-H. Koch, K. Müllen, 'Polyarylenes and Poly(arylenevinylene)s, V. Synthesis of Tetraalkyl-Substituted Oligo(1,4-naphthylene)s and Cyclization to Soluble Oligo(peri-naphthylene)s2)', *Chem. Ber.* **1991**, *124*, 2091–2100.

[75] Q. Peng, Y. Niu, Z. Wang, Y. Jiang, Y. Li, Y. Liu, Z. Shuai, 'Theoretical Predictions of Red and Near-Infrared Strongly Emitting X-Annulated Rylenes', *J. Chem. Phys.* **2011**, *134*, 74510.

[76] L. Flamigni, A. Zanelli, H. Langhals, B. Böck, 'Photophysical and Redox Properties of Perylene Bis- and Tris-Dicarboximide Fluorophores with Triplet State Formation: Transient Absorption and Singlet Oxygen Sensitization', *J. Phys. Chem. A* **2012**, *116*, 1503–1509.

[77] B. Ventura, H. Langhals, B. Bock, L. Flamigni, 'Phosphorescent Perylene Imides', *Chem. Commun.* **2012**, *48*, 4226–4228.

[78] Z. Yu, Y. Wu, Q. Peng, C. Sun, J. Chen, J. Yao, H. Fu, 'Accessing the Triplet State in Heavy-Atom-Free Perylene Diimides', *Chem. - A Eur. J.* **2016**, *22*, 4717–4722.

[79] S. V. Eliseeva, J.-C. G. Bünzli, 'Lanthanide Luminescence for Functional Materials and Bio-Sciences', *Chem. Soc. Rev.* **2010**, *39*, 189–227.

[80] S. Quici, M. Cavazzini, G. Marzanni, G. Accorsi, N. Armaroli, B. Ventura, F. Barigelletti, 'Visible and Near-Infrared Intense Luminescence from Water-Soluble Lanthanide [Tb(III), Eu(III), Sm(III), Dy(III), Pr(III), Ho(III), Yb(III), Nd(III), Er(III)] Complexes', *Inorg. Chem.* **2005**, *44*, 529–537.

[81] L. B. A. Johansson, Y. G. Molotkovsky, L. D. Bergelson, 'Fluorescence and Absorption Properties of Perylenyl and Perylenoyl Probe Molecules in Solvents and Liquid Crystals', *J. Am. Chem. Soc.* **1987**, *109*, 7374–7381.

[82] Z. Yuan, S.-L. Lee, L. Chen, C. Li, K. S. Mali, S. De Feyter, K. Müllen, 'Processable Rylene Diimide Dyes up to 4 nm in Length: Synthesis and STM Visualization', *Chem. Eur. J.* **2013**, *19*, 11842–11846.

[83] M. J. Frisch, G. W. Trucks, H. B. Schlegel, G. E. Scuseria, M. A. Robb, J. R. Cheeseman, G. Scalmani, V. Barone, B. Mennucci, G. A. Petersson, et al., Gaussian 09, Revision A.02, Gaussian, Inc.: Wallingford, CT, **2009**.

[84] A. D. Becke, 'Density-Functional Exchange-Energy Approximation with Correct Asymptotic Behavior', *Phys. Rev. A* **1988**, *38*, 3098–3100.

[85] C. Lee, W. Yang, R. Parr, 'Development of the Colle-Salvetti correlation-energy formula into a functional of the electron density', *Phys. Rev. B* **1988**, *37*, 785–789.

[86] M. D. Hanwell, D. E. Curtis, D. C. Lonie, T. Vandermeersch, E. Zurek, G. R. Hutchison, 'Avogadro: an advanced semantic chemical editor, visualization, and analysis platform', *J. Cheminform.* **2012**, *4*, 17.

[87] M. E. Casida, M. Huix-Rotllant, 'Progress in Time-Dependent Density-Functional Theory', *Annu. Rev. Phys. Chem* **2012**, *63*, 287–323.

[88] R. L. Martin, 'Natural transition orbitals', *J. Chem. Phys.* **2003**, *118*, 4775–4777.

[89] T. Lu, F. Chen, 'Multiwfn: A multifunctional wavefunction analyzer', *J. Comput. Chem.* **2012**, *33*, 580–592.

[90] T. M. Halasinski, J. L. Weisman, R. Ruiterkamp, T. J. Lee, F. Salama, M. Head-Gordon, 'Electronic Absorption Spectra of Neutral Perylene ($C_{20}H_{12}$), Terrylene ($C_{30}H_{16}$), and Quaterrylene ($C_{40}H_{20}$) and Their Positive and Negative Ions: Ne Matrix-Isolation Spectroscopy and Time-Dependent Density Functional Theory Calculations', *J. Phys. Chem. A* **2003**, *107*, 3660–3669.

[91] S. Couris, E. Koudoumas, A. A. Ruth, S. Leach, 'Concentration and Wavelength Dependence of The Effective Third-Order Susceptibility and Optical Limiting of C_{60} In Toluene Solution', *J. Phys. B At. Mol. Opt. Phys.* **1995**, *28*, 4537–4554.

[92] E. Koudoumas, M. Konstantaki, A. Mavromanolakis, X. Michaut, S. Couris, S. Leach, 'Transient and Instantaneous Third-Order Nonlinear Optical Response of C_{60} and the Higher Fullerenes C_{70}, C_{76} and C_{84}', *J. Phys. B At. Mol. Opt. Phys.* **2001**, *34*, 4983–4996.

[93] R. W. Boyd, *Nonlinear Optics*, **2007**.

[94] R. Rangel-Rojo, S. Yamada, H. Matsuda, D. Yankelevich, 'Large Near-Resonance Third-Order Nonlinearity in an Azobenzene-Functionalized Polymer Film', *Appl.*

Phys. Lett. **1998**, *72*, 1021–1023.

[95] N. Liaros, S. Couris, L. Maggini, F. De Leo, F. Cattaruzza, C. Aurisicchio, D. Bonifazi, 'NLO Response of Photoswitchable Azobenzene-Based Materials', *ChemPhysChem* **2013**, *14*, 2961–2972.

[96] Q. Li, Z. Chi, T. Li, X. Ran, L. Guo, 'Photoresponsive Behavior and Switchable Nonlinear Optical Properties of Langmuir-Blodgett Film Based on Azobenzene Derivatives', *Opt. Express* **2017**, *25*, 11503–11513.

[97] A. Barbieri, E. Bandini, F. Monti, V. K. Praveen, N. Armaroli, 'The Rise of Near-Infrared Emitters: Organic Dyes, Porphyrinoids, and Transition Metal Complexes', *Top. Curr. Chem.* **2016**, *374*, 47.

[98] M. Baroncini, G. Bergamini, P. Ceroni, 'Rigidification Or Interaction-Induced Phosphorescence Of Organic Molecules', *Chem. Commun.* **2017**, *53*, 2081–2093.

[99] L. Ravotto, P. Ceroni, 'Aggregation Induced Phosphorescence of Metal Complexes: From Principles To Applications', *Coord. Chem. Rev.* **2017**, *346*, 62–76.

[100] K. Kam-Wing Lo, S. Po-Yam Li, 'Utilization of the Photophysical and Photochemical Properties of Phosphorescent Transition Metal Complexes in the Development of Photofunctional Cellular Sensors, Imaging Reagents, and Cytotoxic Agents', *RSC Adv.* **2014**, *4*, 10560–10585.

[101] H. Xiang, J. Cheng, X. Ma, X. Zhou, J. J. Chruma, 'Near-Infrared Phosphorescence: Materials and Applications', *Chem. Soc. Rev.* **2013**, *42*, 6128–6185.

[102] M. Schulze, A. Steffen, F. Würthner, 'Near-IR Phosphorescent Ruthenium (II) and Iridium (III) Perylene Bisimide Metal Complexes', *Angew. Chem. Inter. Ed.* **2015**, *54*, 1570–1573.

[103] A. Kremer, C. Aurisicchio, F. De Leo, B. Ventura, J. Wouters, N. Armaroli, A. Barbieri, D. Bonifazi, 'Walking Down the Chalcogenic Group of the Periodic Table: From Singlet to Triplet Organic Emitters', *Chem. - A Eur. J.* **2015**, *21*, 15377–15387.

[104] A. Kremer, A. Fermi, N. Biot, J. Wouters, D. Bonifazi, 'Supramolecular Wiring of Benzo-1,3-chalcogenazoles through Programmed Chalcogen Bonding Interactions', *Chem. Eur. J.* **2016**, *22*, 5665–5675.

Entry for the Table of Contents